ACS OMEGA

Open Access

http://pubs.acs.org/journal/acsodf

Article

A Salt Bridge and Disulfide Bond within the Lassa Virus Fusion Domain Are Required for the Initiation of Membrane Fusion

Hallie N. Pennington, Daniel Birtles, Zoe W. Shi, and Jinwoo Lee*

Cite This: *ACS Omega* 2024, 9, 4920−4930

Read Online

ACCESS | Metrics & More | Article Recommendations | Supporting Information

ABSTRACT: Infection with Lassa virus (LASV), an Old-World arenavirus that is endemic to West Africa, causes Lassa fever, a lethal hemorrhagic fever. Delivery of LASV's genetic material into the host cell is an integral component of its lifecycle. This is accomplished via membrane fusion, a process initiated by a hydrophobic sequence known as the fusion domain (FD). The LASV FD (G^{260}−N^{295}) consists of two structurally distinct regions: an N-terminal fusion peptide (FP: G^{260}−T^{274}) and an internal fusion loop (FL: C^{279}−N^{295}) that is connected by a short linker region (P^{275}−Y^{278}). However, the molecular mechanisms behind how the LASV FD initiates fusion remain unclear. Here, we demonstrate that the LASV FD adopts a fusogenic, helical conformation at a pH akin to that of the lysosomal compartment. Additionally, we identified a conserved disulfide bond (C^{279} and C^{292}) and salt bridge (R^{282} and E^{289}) within the FL that are pertinent to fusion. We found that the disulfide bond must be present so that the FD can bind to the lipid bilayer and subsequently initiate fusion. Moreover, the salt bridge is essential for the secondary structure of the FD such that it can associate with the lipid bilayer in the proper orientation for full functionality. In conclusion, our findings indicate that the LASV FD preferentially initiates fusion at a pH akin to that of the lysosome through a mechanism that requires a conserved salt bridge and, to a lesser extent, an intact disulfide bond within the internal FL.

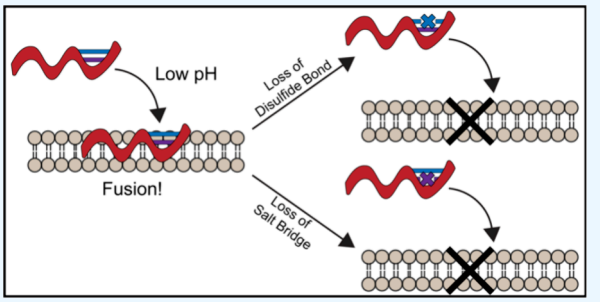

INTRODUCTION

Lassa virus (LASV), an arenavirus endemic to West Africa, has been deemed by the World Health Organization (WHO) as one of the top five diseases requiring prioritized research and development due to its pandemic potential.[1] Infection with LASV causes Lassa fever, a viral hemorrhagic fever that affects an estimated 100,000 to 300,000 individuals, annually, but these numbers may be much higher due to poor healthcare infrastructure in endemic regions.[2−5] In severe cases, the case fatality rate (CFR) of LASV averages around 20%. LASV is primarily spread by direct contact with infected rodent excrement, though there has been an increased incidence of direct human-to-human transmission.[6] Despite these damning statistics and the high pathogenicity of LASV, there are currently no FDA-approved vaccines or antivirals for the explicit treatment of Lassa fever.[7−9] Thus, it is evident that LASV presents a major threat to global public health, especially considering its evolving pathogenicity, as it nears a complete zoonotic jump.

Delivery of LASV's genetic material into the host cell is an integral component of its lifecycle. Since LASV is an enveloped virus, this is accomplished via membrane fusion, which is mediated by the glycoprotein complex (GPC), the sole protein located on the virion surface.[10−12] The GPC comprises a receptor binding subunit (glycoprotein 1, GP1) and a fusion subunit (glycoprotein 2, GP2) that is associated with a stable signal peptide (SSP) [Figure 1]. The initial interaction of GP1 with its primary receptor on the host cell plasma membrane, α-dystroglycan (αDG), has been well studied.[13−15] After engagement with this receptor, the virion is subsequently endocytosed, where fusion ultimately takes place. Notably, the most prominent environmental change in the endocytic pathway is that of decreasing pH, with the early endosome shown to have a pH of 6.5−6.0, the late endosome a pH of 5.5−5.0, and the lysosome a pH of 4.5−4.0.[16] Intriguingly, LASV has been reported to initiate fusion at a pH below 5.0, which is an unusually acidic pH, and suggests that LASV fusion may occur at the late endosomal or lysosomal compartment, although a specific preference has not been discerned.[17−19]

It is believed that LASV follows the six-helix bundle mechanism to mediate membrane fusion, similar to the process undergone by other class one fusion proteins, including severe acute respiratory syndrome coronavirus 2 (SARS-CoV-2), influenza, human immunodeficiency virus (HIV), and Ebola virus (EBOV). Therefore, the initial step of LASV-mediated membrane fusion likely involves the

Received: October 31, 2023
Revised: December 13, 2023
Accepted: December 28, 2023
Published: January 18, 2024

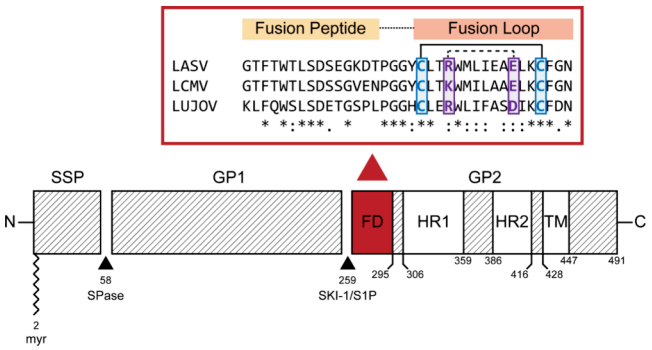

Figure 1. Several regions within the LASV glycoprotein complex (GPC) that have functional relevance to membrane fusion. The GPC is cleaved by SPase at position 58, yielding the stable signal peptide (SSP), which has a myristoylation motif (myr) at position 2, and receptor binding subunit (glycoprotein 1, (GP1)). Following cleavage by SKI-1/S1P at position 259, the fusion subunit (glycoprotein 2, (GP2)) is separated from GP1, releasing a fusion domain (FD, red) at the N-terminus that is composed of two structurally distinct regions: a fusion peptide (FP, yellow) and internal fusion loop (FL, orange) conjoined by a short linker region (dotted line). A structural alignment with two of the most common arenaviruses afflicting humans revealed that the FL contains a conserved disulfide bond (blue, solid line) and salt bridge (purple, dashed line). Residues with full conservation are indicated by an asterisk (*), whereas those with strong and weak similarities are denoted by a semicolon (:) and period (.), respectively. Abbreviations: LCMV, lymphocytic choriomeningitis virus; LUJOV, Lujo virus; HR1, heptad repeat 1; HR2, heptad repeat 2; TM, transmembrane domain.

anchoring of a hydrophobic sequence at the N-terminus of GP2, known as the fusion domain (FD), into the target host cell membrane. This results in the viral and target host cells being tethered together such that membrane fusion can transpire, resulting in the formation of a fusion pore and merging of these membranes. It is thus clear that the FD has an imperative function in viral entry, as it is solely responsible for the initial interaction of LASV with the target host cell membrane. For class one fusion proteins, the FD is generally an N-terminal fusion peptide (FP), like that of HIV and influenza, which have been studied extensively.[20−27] In limited cases, however, viruses contain an internal fusion loop (FL) that is distinguished by a well-conserved disulfide bond, such as that found in EBOV.[28,29] Interestingly, LASV and other arenaviruses, appear to contain both an FP (G^{260}−T^{274}) and FL (C^{279}−N^{295}) within their FD that is connected by a short linker (P^{275}−Y^{278})[30] [Figure 1]. This feature is shared only with coronaviruses, such as SARS-CoV-2, the causative agent of the coronavirus disease-2019 (COVID-19) pandemic. With SARS-CoV-2, it has been demonstrated that the FP and FL are functionally distinct regions that can initiate fusion separately but are most effective in synergy with perturbation of either resulting in a nearly complete hindrance of fusion.[31−37] Nonetheless, the necessity for both the FP and FL within the LASV FD has yet to be established, but given the similarities with the SARS-CoV-2 FD, it can be postulated that these two regions are also functionally distinct and have an important role in the LASV fusion mechanism. However, there has yet to be any detailed investigation into these key functional features concerning the LASV FD.

In this study, we have expressed and purified a 36-amino acid construct that encompasses the complete LASV FD (G^{260}−N^{295}) to investigate the pH conditions and functional features that are pertinent to its fusion mechanism [Figure 1]. Only when the pH was decreased to 4.0 did we witness the adoption of a helical conformation that correlated with a significant increase of FD-initiated fusion, indicating a preference for the lysosomal compartment. Moreover, as there is little information regarding the mechanistic details of the LASV FD, we examined the functional features of its FL, including the disulfide bond (C^{279} and C^{292}) and a salt bridge (R^{282} and E^{289}). Intriguingly, the disulfide bond is not needed to maintain the structure of the FD but is required for association with the target host cell membrane and fusion. Additionally, the salt bridge appears to play a critical role in the fusion mechanism, as its interruption altered the structure of the FD, which, in turn, had an impact on the overall affinity for the membrane and function. Collectively, we demonstrate that the LASV FD has a preference to initiate fusion at a pH resembling that of the lysosomal compartment, which requires an intact disulfide bond and salt bridge for efficient fusion.

MATERIALS AND METHODS

Lipids. 16:0−18:1 1-palmitoyl-2-oleoyl-glycero-3-phosphocholine (POPC), 16:0−18:1 1-palmitoyl-2-oleoyl-*sn*-glycero-3-phospho-[1′-rac-glycerol] (POPG), 18:1 1,2-dioleoyl-*sn*-glycero-3-phosphoethanolamine-*N*-[lissamine rhodamine B sulfonyl] (Rh-PE), and 18:1 1,2-dioleoyl-*sn*-glycero-3-phosphoethanolamine-*N*-[7-nitro-2−1,3-benzoxadiazol-4-yl] (NBD-PE) were all purchased from Avanti Polar Lipids (Alabaster, AL, USA).

Expression. The Lassa virus fusion domain (LASV FD) construct ^{260}(GTFTWTLSDSEGKDTPGGYCLTRWMLIEAELKCFGN)^{295} was designed with an N-terminal 9×-His tag followed by a trp operon leader sequence (TrpLE), and thrombin cleavage site, and then cloned into a pET24*α* vector. Of note, the natural thrombin cleavage site was replaced with LVPR↓GT to yield the native sequence of the LASV FD. The amino acid sequence utilized was derived from a LASV GPC plasmid graciously donated by the Judith M. White lab at the University of Virginia in Charlottesville, Virginia. The LASV FD-containing vector was transformed into *Escherichia coli* strain BL21(DE3)pLysS cells (ThermoFisher Scientific; Waltham, MA, USA). A single colony from the transformation was used to inoculate 5 mL of LB media containing 50 *μ*g/mL kanamycin (ThermoFisher Scientific; Waltham, MA, USA) and 34 *μ*g/mL chloramphenicol (ThermoFisher Scientific; Waltham, MA, USA). This starter culture was grown overnight (approximately 18 h) at 37 °C and 225 rpm in a MaxQ 4000 incubated shaker (ThermoFisher Scientific; Waltham, MA, USA) before being added to 1 L of LB media containing 50 *μ*g/mL kanamycin and 34 *μ*g/mL chloramphenicol. The 1 L culture was grown at 37 °C and 225 rpm until an OD_{600} between 0.6 and 0.8 was achieved, as measured on an Ultrospec 1000 spectrophotometer (Pharmacia Biotech; Cambridge, United Kingdom), and then induced with 1 mM IPTG (ThermoFisher Scientific; Waltham, MA, USA). The culture was incubated for an additional 4 h before being harvested at 4,000 × *g* and 4 °C for 45 min in an Avanti J-15R centrifuge (Beckman Coulter; Brea, CA, USA). The cell pellets were stored at −80 °C or immediately purified. The SARS-CoV-2 fusion domain (SARS-CoV-2 FD) was expressed and purified following the previously described methods.[36]

Purification. The purification protocol previously described by our lab has been adopted and modified to maximize the amount of isolated, pure protein.[38] A 1 L cell pellet

https://doi.org/10.1021/acsomega.3c08632
ACS Omega 2024, 9, 4920−4930

containing the LASV FD was resuspended in 120 mL of sucrose buffer (20% sucrose (w/v), 20 mM Tris, 300 mM NaCl, 10 mM β-mercaptoethanol (BME), 120 μL of Halt protease inhibitor cocktail (ThermoFisher Scientific; Waltham, MA, USA), pH 8.0) and sonicated for 10 min on ice (40% power, 1 s on, 1 s off) with a Branson Digital Sonifier SFX 250 equipped with a titanium flat tip (Emerson; Danbury, CT, USA). After sonication, the solution was then centrifuged at 40,000× g and 4 °C for 1 h via an Avanti J-E centrifuge (Beckman Coulter; Brea, CA, USA). Due to the TrpLE, the target protein was directed to inclusion bodies during expression,[39] which are insoluble in this solution and left in the pellet after this step. Thus, the supernatant was discarded as the target protein was in the pellet, which was then resuspended in 480 mL of lysis buffer (3 M Trichloroacetic acid (TCA), 20 mM Tris, 300 mM NaCl, 10 mM BME, pH 8.0) containing 2% Triton X-100 and 30% glycerol. The solubilized pellet was subsequently sonicated twice (40% power, 1 s on, 1 s off) with a two min rest on ice in between each sonication using a Branson Digital Sonifier SFX 250 equipped with a titanium flat tip (Emerson; Danbury, CT, USA) and then centrifuged at 40,000 × g and 20 °C for 30 min in an Avanti J-E centrifuge (Beckman Coulter; Brea, CA, USA). The supernatant was incubated for at least 24 h with prewashed Ni-NTA resin (Qiagen; Germantown, MD, USA) at 20 °C. Following incubation, the resin was gradient washed in a stepwise fashion with 30 mL per step. The TCA concentration was decreased from 3 to 0 M in 0.75 M increments, BME from 10 to 0 mM in 2.5 mM increments, and glycerol from 30 to 0% in 10% increments using a combination of lysis buffer and salt buffer (20 mM Tris, 300 mM NaCl, pH 8.0). This process gradually removes the lysis buffer and its denaturing components to encourage the LASV FD to properly refold. Upon completion of the gradient wash, the resin was subsequently washed with 300 mL of salt buffer and then 30 mL of cleavage buffer (2.5 mM $CaCl_2$, 20 mM Tris, 100 mM NaCl, pH 8.5). Following this, 5 mg/mL thrombin (BioPharm Laboratories; Bluffdale, UT, USA) was added directly to the LASV FD-bound Ni-NTA resin and brought up to 15 mL with cleavage buffer. The cleavage reaction proceeded for at least 24 h at room temperature while shaking. The flowthrough was collected, and the resin was washed twice with 15 mL of cleavage buffer. The postcleavage flowthrough and washes were pooled together. A representative SDS-PAGE is shown in Figure S1A.

Size Exclusion Chromatography. The pooled postcleavage sample was concentrated with a 3 kDa MWCO Amicon ultra centrifugal filter (Sigma-Aldrich; St. Louis, MO, USA) prior to further purification via size exclusion chromatography (SEC) using a Superdex Peptide 10/30 HR column (Cytiva; Marlborough, MA, USA) with HMA buffer (10 mM HEPES/MES/Sodium Acetate (HMA), 100 mM NaCl, pH 7.4) as the mobile phase and AKTA pure system (Cytiva; Marlborough, MA, USA). A standard curve was prepared for the column utilizing the void (v_o, 4.0 mL) and total volume (v_T, 18.0 mL) of the column as well as the elution volumes (v_e) of cytochrome c (12 384 Da, v_e = 7.1 mL), aprotinin (6512 Da, v_e = 9.2 mL), and vitamin B12 (1355 Da, v_e = 14 mL). The K_{av} of each standard was determined from the equation $\frac{(v_e - v_o)}{(v_t - v_o)}$ and plotted versus the logarithm of the molecular weight. A typical SEC trace is shown in Figure S1B. The fractions containing the isolated protein were then pooled and stored at −80 °C until needed.

Preparation of Unilamellar Vesicles. Large unilamellar vesicles (LUVs) were prepared by mixing appropriate amounts of stock lipid solutions in glass test tubes. Chloroform was removed via gentle vortexing while a continuous nitrogen stream was applied, creating a lipid film. This film was then placed in a vacuum desiccator overnight to further remove residual chloroform. The next day, the lipid film was resuspended in the appropriate volume of HMA buffer via vortexing and subjected to 10 freeze−thaw cycles between liquid nitrogen and a 42 °C water bath and then extruded 21 times through a double layer of 100 nm pore-size polycarbonate membranes (Avestin; Ottawa, ON, CAN). The lipid film for small unilamellar vesicles (SUVs) was prepared similarly to the method described for LUVs; however, after resuspension in the appropriate volume of either CD buffer (1 mM HMA, 10 mM NaCl, pH 7.4) or ITC buffer (10 mM NaOAc, 100 mM NaCl, pH 4.0), the lipids were sonicated on ice for 15 min (1 s on, 1 s off, 10% power) using a Branson Digital Sonifier SFX 250 equipped with a titanium microtip (Emerson; Danbury, CT, USA). The transparent solution was subsequently centrifuged at 20,000 × g for 15 min in an Eppendorf 5425 microcentrifuge (Sigma-Aldrich; St. Louis, MO, USA) to remove any particulates and then transferred to a fresh microcentrifuge tube for usage. All vesicles used in this study were comprised of 65 mol % POPC and 35 mol % POPG unless otherwise indicated.

Fusion Assay. The FRET-based fusion assay outlined here has been frequently employed in the literature to assess the fusion of viral FDs.[23,28,35,40,41] Unlabeled LUVs were mixed with labeled LUVs of 63:35:1:1 POPC:POPG:Rh-PE:NBD-PE at a ratio of 9:1 unlabeled:labeled. Experiments were performed in a Corning Costart black-walled, clear-bottomed 96-well plate (Sigma-Aldrich; St. Louis, MO, USA) with volumes of 150 μL per well containing 100 μM vesicles and 5 μM LASV FD (1:20 protein:lipid) in HMA buffer. HMA buffer is linear from pH 3.0−8.0, as verified via pH titration, so acidification can be carefully controlled through the addition of 1 M HCl. Fluorescence was recorded at 23 °C on a SpectraMax M5 microplate reader (Molecular Devices; San Jose, CA, USA) with excitation and emission wavelengths recorded at 460 and 538 nm, respectively, with a cutoff at 530 nm. For all experiments, the percent fusion was calculated from the equation $\frac{(\mathcal{F}_M - \mathcal{F}_o)}{(\mathcal{F}_\mathcal{T} - \mathcal{F}_o)}$ x 100% where F_M is the measured fluorescence, F_0 is the background fluorescence at pH 7.4, and F_T is the total fluorescence, which was measured after complete vesicle disruption via the addition of 1% Triton X-100. No fusion was witnessed when the FD was incubated at pH 7.4, hence, why this value was used for the background fluorescence. Controls containing no FD were run alongside each experimental condition and subtracted from the final values. Errors were propagated according to the standard error of the mean (SEM).

Circular Dichroism (CD) Spectroscopy. CD measurements were performed on a Jasco J-810 spectrophotometer (Jasco; Easton, MD, USA) with a 2 mm quartz cuvette (Starna Cells; Atascadero, CA, USA). Samples contained 0.8 mM POPC:POPG (65:35) with 20 μM LASV FD (WT) or each mutant. All experiments were carried out at 23 °C in 1 mM HMA, 10 mM NaCl, and pH 4 unless indicated otherwise. For the pH titration, 100 mM HCl was added stepwise until the

https://doi.org/10.1021/acsomega.3c08632
ACS Omega 2024, 9, 4920−4930

desired pH was achieved, which was confirmed with a calibrated pH probe. Spectra were collected from 260 to 198 nm with a step size of 1 at 20 nm/min and averaged over three accumulations. Measurements were taken for the buffer alone containing 0.8 mM SUVs and subtracted from each sample, then smoothed using the program CDToolX.[42] Spectra were converted to mean residue ellipticity (MRE) units and the helical percentage was calculated from the MRE at 222 nm via the following equation: $f_H = \frac{(\theta_{222} - \theta_C)}{(\theta_H - \theta_C)}$, where θ_C = 2,220−53T, θ_H = (250T − 44,000)*(1 − $\frac{3}{n}$), T is the temperature in Celsius, and n is the number of residues in the protein.[28,43,44]

Isothermal Titration Calorimetry (ITC). To prepare the protein for titration, it was placed in a 0.5−3 mL, 3.5 kDa MWCO Slide-A-Lyzer dialysis cassette (ThermoFisher; Waltham, MA, USA), then dialyzed for a minimum of 4 h against 2 L of 10 mM NaOAc, 100 mM NaCl at either pH 5.0 (SARS-CoV-2 ITC buffer) or pH 4.0 (LASV ITC buffer) at 4 °C. The protein was carefully removed from the dialysis cassette and spun down for 15 min at 20,000xg in an Eppendorf 5425 microcentrifuge (Sigma-Aldrich; St. Louis, MO, USA). Following this, the protein was transferred to a clean microcentrifuge tube before being degassed for 8 min in a MicroCal Thermovac (Malvern Panalytical; Malvern, United Kingdom) alongside 20 mM 65:35 POPC:POPG SUVs that were resuspended in the ITC buffer. The protein concentration of the resulting sample was determined following the Pierce BCA protein assay kit microplate reader protocol (ThermoFisher; Waltham, MA, USA), then ran on the ITC. For LASV, the protein concentration was ∼15−20 μM for WT and each mutant, whereas the SARS-CoV-2 FD was 30 μM. All ITC measurements were made using a Malvern VP-ITC microcalorimeter (Malvern Panalytical; Malvern, United Kingdom) in ITC buffer. The sample cell was filled with the degassed protein solution, and the injection syringe with the degassed SUVs. All titrations were performed at 23 °C with 41 injections in total. Each injection was 7 μL with a 16.8 s duration, except for the first injection, which was 2 μL with a 4.8 s duration. For all injections, the reference power was set to 5 μcal/s, and there was an initial delay of 1200 s. The stirring speed was 310 rpm, while the filter period was 2 s. All processing was conducted through NITPIC[45] and SEDPHAT[46] with final figures generated via GUSSI.[47] At least two titrations were performed for each condition with the average K_d and standard deviation presented on each isotherm.

RESULTS

A pH resembling that of the lysosome enhances LASV FD-initiated fusion. To probe the relationship between the pH and functionality of the LASV FD, we employed a FRET-based fusion assay across a range of environmental pH values that are relevant to the endocytic pathway [Figure 2A]. The LASV FD was mixed with vesicles comprised of 65:35 POPC:POPG to provide a simple imitation of the membrane composition found in the late endocytic pathway, where anionic lipids are a key constituent.[48−50] We observed no fusion at a pH resembling that of the plasma membrane (pH 7.4−7.0). Minimal fusion was noted at a pH similar to that of the early endosome (pH 6.5−6.0), which was followed by a slight increase at a pH comparable to the late endosome (pH 5.5−5.0). In contrast, fusion readily occurred at a pH akin to the lysosomal compartment (pH 4.5−4.0). More specifically, a 5-fold increase in fusion was observed between the late endosome (pH 5.0) and lysosome (4.0), whereas a 3-fold increase was noted when the latter was compared to pH 4.5. This indicates that the LASV FD is sensitive to environmental pH and must be shuttled to the late endocytic pathway before any degree of fusion can occur, with the optimal compartment for it to initiate fusion suggested to be the lysosome.

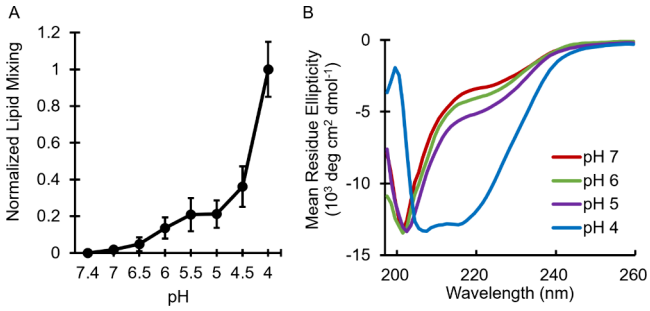

Figure 2. Function and secondary structure of the LASV FD have a large pH dependence. [A] Positive correlation between pH and fusion with optimal fusion occurring at a pH of 4.0, which is akin to the lysosome ($n \geq 6$). Data normalized to pH 4. [B] Global secondary structure is dependent on environmental pH with a helical structure only adopted at pH 4.

To further prove the impact of environmental pH on the LASV FD, we utilized CD spectroscopy to investigate the structural impact of the different physiologically relevant pHs found along the endocytic pathway on the FD. We demonstrate that the global secondary structure of the FD remains unchanged until a pH resembling that of the lysosome (pH 4.0) was introduced [Figure 2B]. From pH 7.0 to 5.0, the LASV FD appeared to exist in a predominantly random coil conformation, as distinguished by the single, negative dip at 200 nm.[51−53] Nonetheless, when we reduced the pH to 4.0, we observed a significant change in the secondary structure of the LASV FD to be mainly an α helix, which was denoted by the double dip at 208 and 222 nm. This was reinforced by size exclusion chromatography (SEC) as there was an increase in the elution volume of the FD when the pH was reduced from 7.4 to 4.0, characteristic of a smaller, more compact structure [Figure S2A].[54] The helical content was calculated to be 35% at pH 4.0, which corresponded to the involvement of nearly 13 residues in the helix. Although we cannot discern the exact location of the helix within the LASV FD, these findings indicate that the structure and function of the LASV FD are pH-dependent, where the FD can only induce fusion at a low pH akin to that found in the lysosomal compartment when it adopts a helical conformation.

The disulfide bond within the FL is important for the interaction of the LASV FD with the lipid membrane and its fusogenicity. To assess the importance of the disulfide bond within the fusion mechanism of the complete LASV FD, we first addressed the ability of the FD to initiate fusion when the disulfide bond was broken. When the reducing agent tris(2-carboxyethyl)phosphine (TCEP) was introduced to eliminate the disulfide bond, we witnessed a significant 3-fold decrease in fusion activity [Figure 3A]. Interestingly, the addition of TCEP to the FD did not impart significant changes to the global secondary structure [Figure 3B]. Furthermore, the helical content of the LASV FD remained relatively unchanged at 37% when TCEP was introduced in comparison

https://doi.org/10.1021/acsomega.3c08632
ACS Omega 2024, 9, 4920−4930

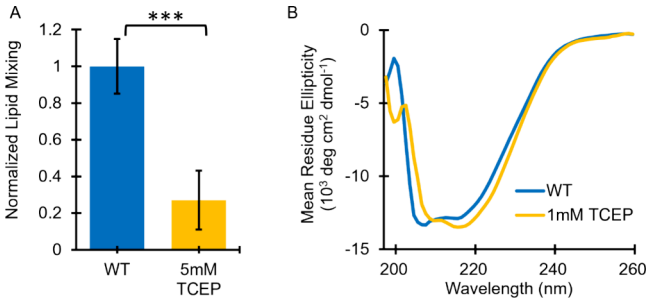

Figure 3. A conserved disulfide bond is required for efficient function of the LASV FD, but not for the global secondary structure. [A] Disruption of the disulfide bond reduced fusion ($n \geq 15$). Data normalized to WT. Student's t-Test assuming unequal variances used to calculate P- value; *** = $P < 0.001$. [B] Global secondary structure remained relatively unchanged under reducing conditions.

to that of the WT at 35%. This was corroborated by SEC where an identical elution volume was noted in the absence and presence of TCEP [Figure S2B]. Thus, the observed loss of function did not appear to be due to a perturbation of the global secondary structure or the oligomeric state of the FD.

We next asked if the loss of functionality was due to an inability of the FD to associate with the vesicles without its conserved disulfide bond. To address this question, we measured the initial interaction of the LASV FD with 65:35 POPC:POPG vesicles in the absence and presence of TCEP via isothermal titration calorimetry (ITC). We have found that the complete FD has a strong affinity for the vesicles with a dissociation constant (K_d) of 11.7 ± 0.8 μM [Figure 4A].[29,55−57] However, when TCEP was introduced, the affinity

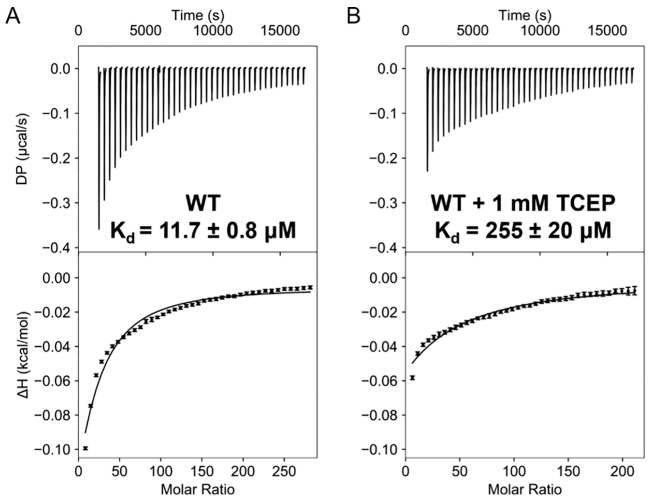

Figure 4. Interruption of the disulfide bond resulted in a decreased binding affinity of the LASV FD. [A] WT and [B] WT with 1 mM TCEP. Both ITC experiments were conducted in 10 mM NaOAc, 100 mM NaCl, pH 4.0 with vesicles titrated into the protein. Dissociation constants (K_d) are displayed on the respective isotherm.

of the FD for the vesicles was significantly hindered, as denoted by the almost 20-fold increase in the K_d to 255 ± 20 μM [Figure 4B]. Put together, our results indicate that the disulfide bond within the FL is imperative for the initial interaction of the LASV FD with the membrane and, thus, its overall function.

A salt bridge within the FL is critical to the overall structure and function of the LASV FD. When assessing the LASV FD, we discovered a potential salt bridge (R^{282} and E^{289}) within the FL. A sequence alignment revealed that the charge distribution of the salt bridge is well conserved where positive and negative residues exist at the same position [Figure 1]. We first aimed to determine if there was any merit behind our notion that the proposed salt bridge has a specific role within LASV FD-initiated membrane fusion. This was accomplished by introducing 500 mM NaCl to the LASV FD, which would ablate any ionic interactions, such as a salt bridge, due to competition between the charged ions and side chains. Interestingly, when high salt concentrations were introduced to the LASV FD, we noted a significant reduction in the amount of fusion [Figure 5A]. In contrast, when the same conditions were applied to the SARS-CoV-2 FD, which was not expected to contain a salt bridge, fusion was affected to a much lesser extent. We then sought to determine how the identified salt bridge may impact the ability of the LASV FD to associate with the vesicles. We observed a decreased affinity of the LASV FD for the vesicles under high salt concentrations, as denoted by the drastic increase in the K_d to 339 ± 12 μM under these conditions [Figure 5B]. Opposingly, under physiological conditions (100 mM NaCl), the SARS-CoV-2 FD had a K_d of 9.9 ± 0.8 μM [Figure 5C], which remained relatively unchanged at 11.8 ± 1.0 μM when the salt concentrations were increased to 500 mM NaCl [Figure 5D]. Thus, it is clear that the LASV FD, but not the SARS-CoV-2 FD, is sensitive to high salt concentrations, indicating that a salt bridge likely exists in the LASV FD.

To investigate the role of the individual residues within the salt bridge in LASV FD-initiated membrane fusion, we generated single-point mutants (i.e., $R^{282}E$ and $E^{289}R$) as well as a double mutant ($R^{282}E/E^{289}R$). The selected single-point mutations should prevent the formation of the salt bridge as both residues would now carry the same charge (i.e., $R^{282}E$ and E^{289} vs R^{282} and $E^{289}R$). Theoretically, the double mutation should maintain the salt bridge as the positioning of the residues would merely be switched. For each mutant, we observed a dramatic reduction in fusion in comparison to WT [Figure 6A], which was partially due to a decrease in binding affinity [Figure S3]. The $R^{282}E/E^{289}R$ and $R^{282}E$ mutants had a nearly identical effect on function where either mutation resulted in a 4-fold decrease in fusion and a 15-fold increase in the K_d. Specifically, the $R^{282}E/E^{289}R$ mutant had a K_d of 158 ± 21 μM [Figure S3A] whereas the $R^{282}E$ mutant had a K_d of 181 ± 17 μM [Figure S3B]. Surprisingly, the $E^{282}R$ mutation had a more significant impact with a 10-fold reduction in fusion and a vast, 40-fold increase in the K_d to 414 ± 19 μM [Figure S3C] in contrast to WT. Intriguingly, when 500 mM NaCl was introduced to $R^{282}E/E^{289}R$, there was a significant decrease in its ability to initiate fusion, whereas there was no substantial difference in the ability of either single mutant ($R^{282}E$ or $E^{289}R$) to initiate fusion under physiological or high salt conditions [Figure S4].

We next examined the secondary structure of each mutant and found that all three were perturbed in comparison to the WT [Figure 6B]. More specifically, the $R^{282}E$ mutant appeared to adopt a mixture of secondary structures as denoted by deep dips at 208 and 222 nm, indicative of a helix, and minimum near 215 nm, suggestive of a β-sheet conformation.[51] The $E^{289}R$ mutant seemed to shift the conformation back to a largely random coil structure, as indicated by the decrease in

https://doi.org/10.1021/acsomega.3c08632
ACS Omega 2024, 9, 4920−4930

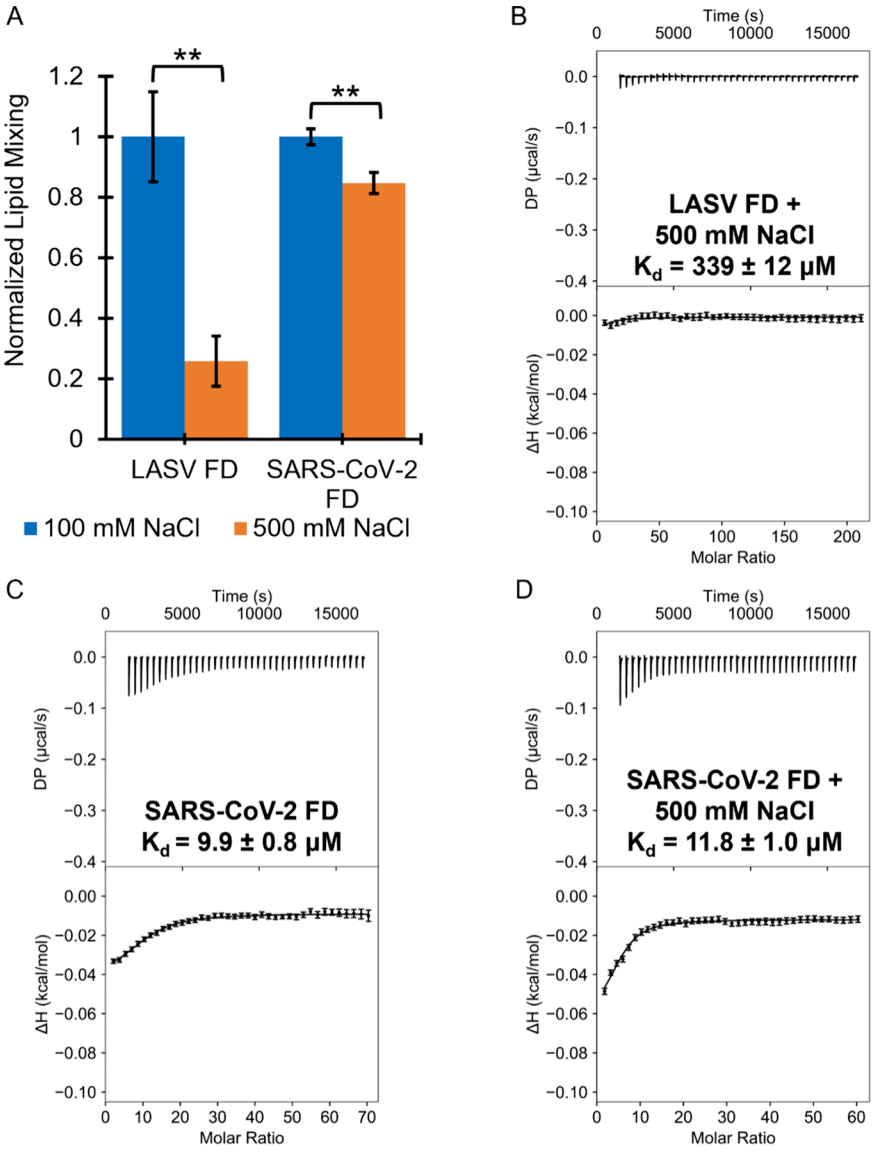

Figure 5. High salt concentrations impair the functionality of the LASV FD, but not the SARS-CoV-2 FD. [A] Introduction of 500 mM NaCl to the buffer system significantly reduced fusion for the LASV FD, but not SARS-CoV-2 FD ($n \geq 18$). Data normalized to 100 mM NaCl for each FD. Student's t-Test assuming unequal variances used to calculate P-value; ** = $P < 0.01$, *** = $P < 0.001$. [B] LASV FD with 500 mM NaCl; [C] SARS-CoV-2 FD; and [D] SARS-CoV-2 FD with 500 mM NaCl. All ITC experiments conducted in 10 mM NaOAc, 100 mM NaCl or 500 mM NaCl at pH 5.0 (SARS-CoV-2) or pH 4.0 (LASV), with vesicles titrated into the protein. Dissociation constants (K_d) are displayed on the respective isotherm.

intensity at 222 and 208 nm and the appearance of a deep minimum near 200 nm. For the $R^{282}E/E^{289}R$ mutant, we witnessed a decrease in intensity at 222 nm, but the 208 nm intensity was similar to that observed for the WT, correlating to a decrease in helical content to 30% and fewer residues involved in the helical structure. Notably, SEC demonstrated that each salt bridge mutant remained monomeric at both physiological pH [Figure S5A] and low pH [Figure S5B]. It is therefore apparent from our data that the identified salt bridge is integral to the LASV FD as its perturbation has a significant impact on both the overall function and structure. Moreover, it is evident that both charges of the salt bridge are indispensable, but the local impact of the residue at position 289 (E^{289}) is greater than the residue at position 282 (R^{289}).

DISCUSSION

LASV is an emerging arenavirus that has no FDA-approved vaccines or antivirals despite an increased incidence of human-to-human transmission. Delivery of LASV's genetic material into the host cell is an integral component of its lifecycle and is achieved via membrane fusion, a process that is initiated by the FD. While the FD of most class one fusion proteins contains only an FP or FL, the LASV FD is unique in that it contains both an FP and FL in tandem. Despite this distinctive characteristic, little is known about the LASV FD, particularly the membrane where it initiates fusion and any functional components that are important toward this process. Here, we indicate that the LASV FD has a distinct preference to initiate fusion at an environmental pH akin to that of the lysosomal membrane, at which point it adopts a fusogenic, helical conformation. We reveal that both a disulfide bond and salt

https://doi.org/10.1021/acsomega.3c08632
ACS Omega 2024, 9, 4920−4930

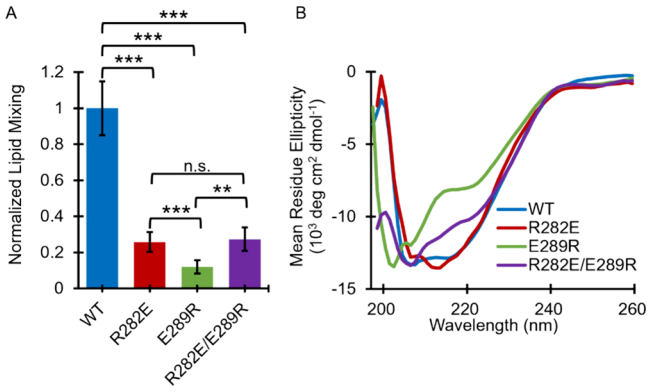

Figure 6. An identified salt bridge is critical to the overall structure and function of the LASV FD. [A] Under physiological salt conditions (100 mM NaCl), all salt bridge mutants ($R^{282}E$, red; $E^{289}R$, green; $R^{282}E/E^{289}R$, purple) had decreased fusion in comparison to WT (blue) ($n \geq 38$). All lipid mixing normalized to WT, pH 4. Student's *t* test assuming unequal variances used to calculate P-value; n.s. = not significant, ** = $P < 0.01$, and *** = $P < 0.001$. [B] Mutation of any salt bridge residue altered the secondary structure.

bridge within the FL must be present for the LASV FD to interact with the target membrane and efficiently mediate fusion.

In the literature, LASV-mediated membrane fusion has been demonstrated to be a pH-dependent process and promoted by the engagement of GP1 with a secondary, intracellular receptor late within the endocytic pathway, known as lysosomal associated membrane protein 1 (LAMP1).[17−19,58−60] To date, however, the specific conditions that trigger the fusion machinery, particularly the LASV FD, remain unclear. Furthermore, any conformational changes undergone by the LASV FD have not been discerned even though other viral FDs will undergo a structural transition to adopt a more fusogenic conformation, often becoming α-helical, when triggered to initiate fusion.[28,32,55,61,62] For example, in the EBOV FD, the helical content becomes increased at a low pH, a conformational change that is required to mediate fusion.[28,29,55] The HIV FD must also undergo a conformational change to initiate fusion, predominantly becoming more helical.[23,63] In a simplistic membrane model, our findings demonstrate that the complete LASV FD has a clear pH dependency in its ability to initiate fusion with optimal fusion suggested to occur at pH 4.0 [Figure 2A], which is directly linked to conformational changes [Figure 2B, S2A]. We believe that the α-helical conformation we witnessed at pH 4.0 is the fusogenic form of the LASV FD, whereas the random coil seen at higher pH was the nonfusogenic form. Our ITC experiments support this notion as the FD had a strong affinity for the lipid bilayer at pH 4.0, but no affinity at pH 7.0 [Figure S6]. Intriguingly, MD simulations indicated that the FD adopts a random coil structure at pH 5.5 that was capable of inserting into the membrane.[64] This could potentially explain why we witnessed some fusion at a pH similar to the late endosome as the FD could perturb the lipid bilayer but did not have the proper orientation to make preferential interactions such that fusion could be initiated efficiently. In turn, we anticipate that the helical conformation adopted by the FD at pH 4.0 likely allows for favorable hydrophobic interactions with the target host cell membrane, specifically the lysosomal membrane, such that membrane fusion can be initiated. While it could be suggested that GP1 dissociation or LAMP1-binding may slightly alter this optimal pH, our data indicate that pH 4.0 is an essential requirement for the FD to undergo the conformational change necessary to initiate fusion. Collectively, this reinforces the idea that LASV must enter the endocytic pathway with optimal fusion occurring at the lysosomal compartment after the FD adopts the fusogenic, helical conformation and is independent of GP1 dissociation or LAMP1 engagement.

Despite its critical role in the initial interaction with the target host cell membrane, the LASV FD has received limited attention in previous studies, particularly its functional components. In our investigation of LASV FD-initiated membrane fusion, we have uncovered that an intact disulfide bond within the LASV FL is essential for the full functionality of the complete FD [Figure 3A]. One plausible explanation would be that the disulfide bond provided structural stabilization of the LASV FD, particularly its folding or oligomeric state, such that the helical conformation adopted at a low pH is maintained and fusion can occur. This notion is supported by the EBOV FD and baculovirus FD, both of which characteristically contain an FL, where disruption of the disulfide bond resulted in conformational changes that impacted fusion.[16,65−67] However, for the LASV FD, the global secondary structure [Figure 3B] remained relatively unchanged under the reducing conditions. It could be argued that the oligomeric state of the LASV FD was affected without an intact disulfide bond, but the introduction of reducing conditions brought about no change in the SEC trace [Figure S2B], correlating to monomeric states for both. Thus, we postulate that disruption of the disulfide bond affected the tertiary structure of the LASV FD. Furthermore, our findings indicate that this alteration interfered with the initial interaction of the LASV FD with the target membrane, which, with the disulfide bond present, had a K_d akin to those of other class one fusion proteins that increased significantly (20-fold) when the cysteines were reduced [Figure 4].[29,55−57] Intriguingly, this finding aligned with literature regarding the SARS-CoV-2 FD, which also features both an FP and FL in tandem, where the disulfide bond within the FL was demonstrated to have an explicit, vital role in the fusion mechanism.[31−35,37] Specifically, the overall secondary structure of the SARS-CoV-2 FD was maintained without the disulfide bonded FL, but there was a large and significant decrease in fusogenicity, postulated to be due to a change in the tertiary structure that altered its ability to associate/interact with the target host cell membrane and/or the FP. Taken together, this indicates that the LASV FD is capable of forming the helical conformation in the absence of the disulfide bond in the FL, but was not able to effectively associate with the target host cell membrane, resulting in the reduction of fusion efficiency.

During our investigation of the key functional features of FL within the LASV FD, we identified a potential salt bridge that may be important for fusion. A sequence alignment of the LASV FD alongside other notable family members indicated that charged residues were highly conserved in the same position, specifically R^{282} and E^{289}, suggestive of a salt bridge [Figure 1]. This was supported by a recent Cryo-EM structure of the prefusion LASV GPC which placed the side chains of these two residues within 4.4 to 5.5 Å, where a strong salt bridge has been shown to have an optimal distance of ∼4.5 Å.[68−70] We show that high salt concentrations resulted in a significant, 4-fold (75%) decrease in fusion [Figure 5A] and an inability to associate with the lipid bilayer [Figure 5B] in

https://doi.org/10.1021/acsomega.3c08632
ACS Omega 2024, 9, 4920−4930

comparison to the LASV FD under physiological conditions. It could be claimed that this observation was due to an interaction between the anionic lipids of our vesicles and the salt ions, hindering association with the target host cell membrane and/or function of the FD. Therefore, we carried out the same set of experiments on the SARS-CoV-2 FD, where a potential salt bridge was not apparent. We establish that high salt concentrations had a minimal impact on the ability of the SARS-CoV-2 FD to associate with the lipid bilayer [Figure 5C,D], but moderate loss of fusion (15%); albeit to a much lesser extent than the LASV FD. We theorize that this was due to indirect competition between the SARS-CoV-2 FD and salt ions for nonspecific interactions with water molecules or anionic lipids, resulting in a depletion of the hydration barrier of the protein and/or masking of the lipid bilayer charge, respectively.[68,69,71−73] Nonspecific interactions contribute to membrane fusion significantly less than specific interactions that have structural and functional relevance, such as the salt bridge elucidated within the LASV FD, providing a rationalization for the decrease in fusion observed for the SARS-CoV-2 FD despite its ability to associate with the lipid bilayer. Nonetheless, we postulate that there was a direct competition between the LASV FD and salt ions for specific ionic interactions, which resulted in the ablation of the salt bridge. Even when accounting for the reduction in fusion caused by general, nonspecific interactions in high salt concentrations, we still witnessed a significant 2.5-fold (60%) decrease in fusion by the LASV FD. Collectively, this gives credence to our hypothesis that the identified salt bridge was a unique feature of the LASV FD and required for association with the lipid bilayer such that there is full functionality.

Single mutants were created such that both residues within the salt bridge carried the same charge (i.e., $R^{282}E$ and $E^{289}R$) as well as a double mutant that switched the positioning of the charges (i.e., $R^{282}E/E^{289}R$). We hypothesized that the single mutants would ablate the salt bridge due to the existence of the same charge at either position, which would impede the necessary ionic interaction and result in decreased function or structural perturbations. In turn, we believed that any functional and/or structural impacts could be rescued by the double mutant, as the required residues for the ionic interaction would be present, albeit at swapped positions, such that the salt bridge would be restored. Unexpectedly, we observed a significant decrease in the binding affinity and, subsequently, fusogenicity for all three mutants in comparison to WT [Figure 6A, S4]. Additionally, the secondary structure but not the oligomeric state was perturbed for each mutant [Figure 6B, S5]. Based on our findings, a possible explanation is that the disruption of the salt bridge between the side chains of the basic residue at position 282 (R^{282}) and the acidic residue at position 289 (E^{289}) has a critical role in LASV FD-initiated membrane fusion. Specifically, upon the delivery of LASV to the lysosomal compartment, the low pH environment causes the side chain of E^{289} within the FD to become protonated. This breaks the salt bridge, which results in the formation of a new bonding network within the LASV FD, prompting adoption of the fusogenic, helical conformation necessary for the initiation of fusion. Here, we believe that R^{282} forms new interactions, which stabilize the fusogenic conformation of the FD. Our data supports this notion as both single mutants had decreased fusion and altered secondary structures where mutation of $E^{289}R$ was particularly devastating with a largely random coil structure at low pH [Figure 6]. Moreover, the salt bridge was likely reformed in the double mutant ($R^{282}E/E^{289}R$), as indicated by the significant decrease in fusion under high salt concentrations [Figure S4]. However, switching the charges still disrupted the overall bonding network, preventing the formation of the proper fusogenic helical structure required for efficient fusion. Thus, the position of the charge appears to be imperative to the function of the LASV FD. This is in alignment with previous studies, where ionic interactions are suggested to sense the pH and form a proper conformation to ensure membrane fusion occurs at the appropriate location.[74−80]

In summary, our data indicate that the LASV FD has a distinct preference to mediate fusion at a pH that is akin to the lysosomal compartment, which is directly linked to the adoption of a fusogenic, helical conformation. In a simplistic model, we have illustrated that the helical conformation alone is insufficient to have a robust interaction with the target host cell membrane and initiate fusion. Here, two bonds within the FL of the LASV FD have been demonstrated to play an important role in this action: the disulfide bond located between C^{279} and C^{292} as well as the salt bridge that occurs between R^{282} and E^{289}. In particular, an intact disulfide bond is necessary for the LASV FD to efficiently bind to the target host cell membrane. Additionally, the salt bridge must be present to maintain the global secondary structure and behaves as a potential pH-sensing site that allows the FD to initiate fusion in the appropriate compartment. Overall, we have provided a deeper understanding of the molecular mechanisms that influence LASV FD-initiated membrane fusion as well as more general insights into the functional roles of the FL within LASV fusion. These critical components have the potential to serve as a therapeutic target for the development of a novel antiviral to target the FD and prevent membrane fusion, such that LASV infection cannot occur. In the future, the investigation of more complex lipids is warranted to gain a better understanding of physiologically relevant lipid compositions toward FD-initiated membrane fusion and therapeutic development.

■ ASSOCIATED CONTENT

Supporting Information

The Supporting Information is available free of charge at https://pubs.acs.org/doi/10.1021/acsomega.3c08632.

Expression and purification of the Lassa virus fusion domain, SEC of the LASV FD at relevant pHs (physiological and lysosomal) as well as under reducing conditions, exemplary isotherms of salt bridge mutants of LASV FD, fusion assay of salt bridge mutants of LASV FD under physiological and high salt concentrations, SEC of salt bridge mutants at physiological and lysosomal pH, and exemplary isotherm of LASV FD at physiological pH (PDF)

■ AUTHOR INFORMATION

Corresponding Author

Jinwoo Lee − *Department of Chemistry and Biochemistry, College of Computer, Mathematics, and Natural Science, University of Maryland College Park, College Park, Maryland 20740, United States;* orcid.org/0000-0002-1433-2810; Email: jinwoo@umd.edu

https://doi.org/10.1021/acsomega.3c08632
ACS Omega 2024, 9, 4920−4930

Authors

Hallie N. Pennington − *Department of Chemistry and Biochemistry, College of Computer, Mathematics, and Natural Science, University of Maryland College Park, College Park, Maryland 20740, United States;* orcid.org/0000-0003-1192-3057

Daniel Birtles − *Department of Chemistry and Biochemistry, College of Computer, Mathematics, and Natural Science, University of Maryland College Park, College Park, Maryland 20740, United States;* orcid.org/0000-0001-6589-8526

Zoe W. Shi − *Department of Chemistry and Biochemistry, College of Computer, Mathematics, and Natural Science, University of Maryland College Park, College Park, Maryland 20740, United States*

Complete contact information is available at: https://pubs.acs.org/10.1021/acsomega.3c08632

Author Contributions

H.N.P., D.B., and J.L. designed the experiments. H.N.P performed the LASV experiments and was supported by Z.W.S. D.B. carried out the SARS-CoV-2 experiments. H.N.P. and D.B. analyzed the data. H.N.P. and J.L. prepared the manuscript.

Funding

This work was supported by the National Science Foundation (CHE-2238139).

Notes

The authors declare no competing financial interest.

■ ACKNOWLEDGMENTS

We would like to express our gratitude to all lab members for their help in editing this manuscript.

■ REFERENCES

(1) Mehand, M. S.; Al-Shorbaji, F.; Millett, P.; Murgue, B. The WHO R&D Blueprint: 2018 review of emerging infectious diseases requiring urgent research and development efforts. *Antiviral Res.* **2018**, *159*, 63−67.

(2) Richmond, J. K.; Baglole, D. J. Lassa fever: epidemiology, clinical features, and social consequences. *British Medical Journal* **2003**, *327* (7426), 1271−1275.

(3) McCormick, J. B.; Webb, P. A.; Krebs, J. W.; Johnson, K. M.; Smith, E. S. A Prospective Study of the Epidemiology and Ecology of Lassa Fever. *J. Infect. Diseases* **1987**, *135* (3), 437−444.

(4) Lecompte, E.; Fichet-Calvet, E.; Daffis, S.; Koulémou, K.; Sylla, O.; Kourouma, F.; Doré, A.; Soropogui, B.; Aniskin, V.; Allali, B.; et al. Mastomys natalensis and Lassa fever, West Africa. *Emerging Infectious Diseases* **2006**, *12* (12), 1971−1974.

(5) Safronetz, D.; Lopez, J. E.; Sogoba, N.; Traore', S. F.; Raffel, S. J.; Fischer, E. R.; Ebihara, H.; Branco, L.; Garry, R. F.; Schwan, T. G.; Feldmann, H.; et al. Detection of Lassa virus. *Mali. Emerging Infect. Dis.* **2010**, *16* (7), 1123−1126.

(6) World Health Organization. *Lassa Fever - United Kingdom of Great Britain and Northern Ireland*. https://www.who.int/emergencies/disease-outbreak-news/item/lassa-fever-united-kingdom-of-great-britain-and-northern-ireland (accessed.

(7) Mire, C. E.; Cross, R. W.; Geisbert, J. B.; Borisevich, V.; Agans, K. N.; Deer, D. J.; Heinrich, M. L.; Rowland, M. M.; Goba, A.; Momoh, M.; et al. Human-monoclonal-antibody therapy protects nonhuman primates against advanced Lassa fever. *Nature Medicine* **2017**, *23* (10), 1146−1149.

(8) Eberhardt, K. A.; Mischlinger, J.; Jordan, S.; Groger, M.; Günther, S.; Ramharter, M. Ribavirin for the treatment of Lassa fever: A systematic review and meta-analysis. *International Journal of Infectious Diseases* **2019**, *87*, 15−20.

(9) McCormick, J. B.; King, I. J.; Webb, P. A.; Scribner, C. L.; Craven, R. B.; Johnson, K. M.; Elliott, L. H.; Belmont-Williams, R. Lassa fever. Effective therapy with ribavirin. *New England Journal of Medicine* **1986**, *314* (1), 20−26.

(10) Pennington, H. N.; Lee, J. Lassa virus glycoprotein complex review: insights into its unique fusion machinery. *Biosci. Rep.* **2022**, *42* (2), No. BSR20211930, DOI: 10.1042/BSR20211930.

(11) Hastie, K. M.; Zandonatti, M. A.; Kleinfelter, L. M.; Heinrich, M. L.; Rowland, M. M.; Chandran, K.; Branco, L. M.; Robinson, J. E.; Garry, R. F.; Saphire, E. O. Structural basis for antibody-mediated neutralization of Lassa virus. *Science* **2017**, *356* (6341), 923.

(12) Katz, M.; Weinstein, J.; Eilon-Ashkenazy, M.; Gehring, K.; Cohen-Dvashi, H.; Elad, N.; Fleishman, S. J.; Diskin, R. Structure and receptor recognition by the Lassa virus spike complex. *Nature* **2022**, *603* (7899), 174−179.

(13) Oppliger, J.; Torriani, G.; Herrador, A.; Kunz, S. Lassa Virus Cell Entry via Dystroglycan Involves an Unusual Pathway of Macropinocytosis. *J. Virol* **2016**, *90* (14), 6412−6429.

(14) Cao, W.; Henry, M. D.; Borrow, P.; Yamada, H.; Elder, J. H.; Ravkov, E. V.; Nichol, S. T.; Compans, R. W.; Campbell, K. P.; Oldstone, M. B. A. Identification of α-Dystroglycan as a Receptor for Lymphocytic Choriomeningitis Virus and Lassa Fever Virus. *Science* **1998**, *282* (5396), 2079−2081.

(15) Acciani, M.; Alston, J. T.; Zhao, G.; Reynolds, H.; Ali, A. M.; Xu, B.; Brindley, M. A. Mutational Analysis of Lassa Virus Glycoprotein Highlights Regions Required for Alpha-Dystroglycan Utilization. *J. Virol* **2017**, *91* (18), 10 DOI: 10.1128/JVI.00574-17.

(16) White, J.; Whittaker, G. Fusion of Enveloped Viruses in Endosomes. *Traffic* **2016**, *17* (6), 593−614.

(17) Bulow, U.; Govindan, R.; Munro, J. B. Acidic pH Triggers Lipid Mixing Mediated by Lassa Virus GP. *Viruses* **2020**, *12* (7). DOI: 716.

(18) Cosset, F. L.; Marianneau, P.; Verney, G.; Gallais, F.; Tordo, N.; Pécheur, E. I.; ter Meulen, J.; Deubel, V.; Bartosch, B. Characterization of Lassa virus cell entry and neutralization with Lassa virus pseudoparticles. *J. Virol* **2009**, *83* (7), 3228−3237.

(19) Klewitz, C.; Klenk, H. D.; ter Meulen, J. Amino acids from both N-terminal hydrophobic regions of the Lassa virus envelope glycoprotein GP-2 are critical for pH-dependent membrane fusion and infectivity. *J. Gen. Virol.* **2007**, *88* (Pt 8), 2320−2328.

(20) Dimitrov, A. S.; Rawat, S. S.; Jiang, S.; Blumenthal, R. Role of the fusion peptide and membrane-proximal domain in HIV-1 envelope glycoprotein-mediated membrane fusion. *Biochemistry* **2003**, *42* (48), 14150−14158.

(21) Han, X.; Bushweller, J. H.; Cafiso, D. S.; Tamm, L. K. Membrane structure and fusion-triggering conformational change of the fusion domain from influenza hemagglutinin. *Nat. Struct. Biol.* **2001**, *8* (8), 715−720.

(22) Li, Y.; Tamm, L. K. Structure and plasticity of the human immunodeficiency virus gp41 fusion domain in lipid micelles and bilayers. *Biophys. J.* **2007**, *93* (3), 876−885.

(23) Lai, A. L.; Moorthy, A. E.; Li, Y.; Tamm, L. K. Fusion activity of HIV gp41 fusion domain is related to its secondary structure and depth of membrane insertion in a cholesterol-dependent fashion. *J. Mol. Biol.* **2012**, *418* (1−2), 3−15.

(24) Yang, S. T.; Kiessling, V.; Simmons, J. A.; White, J. M.; Tamm, L. K. HIV gp41-mediated membrane fusion occurs at edges of cholesterol-rich lipid domains. *Nat. Chem. Biol.* **2015**, *11* (6), 424−431.

(25) Gray, C.; Tatulian, S. A.; Wharton, S. A.; Tamm, L. K. Effect of the N-terminal glycine on the secondary structure, orientation, and interaction of the influenza hemagglutinin fusion peptide with lipid bilayers. *Biophys. J.* **1996**, *70* (5), 2275−2286.

(26) Gething, M. J.; Doms, R. W.; York, D.; White, J. Studies on the mechanism of membrane fusion: site-specific mutagenesis of the hemagglutinin of influenza virus. *J. Cell Biol.* **1986**, *102* (1), 11−23.

(27) Smrt, S. T.; Draney, A. W.; Lorieau, J. L. The influenza hemagglutinin fusion domain is an amphipathic helical hairpin that

functions by inducing membrane curvature. *J. Biol. Chem.* **2015**, *290* (1), 228−238.
(28) Gregory, S. M.; Harada, E.; Liang, B.; Delos, S. E.; White, J. M.; Tamm, L. K. Structure and function of the complete internal fusion loop from Ebolavirus glycoprotein 2. *Proc. Natl. Acad. Sci. U. S. A.* **2011**, *108* (27), 11211−11216.
(29) Gregory, S. M.; Larsson, P.; Nelson, E. A.; Kasson, P. M.; White, J. M.; Tamm, L. K. Ebolavirus entry requires a compact hydrophobic fist at the tip of the fusion loop. *J. Virol* **2014**, *88* (12), 6636−6649.
(30) Glushakova, S. E.; Lukashevich, I. S.; Baratova, L. A. Prediction of arenavirus fusion peptides on the basis of computer analysis of envelope protein sequences. *FEBS Lett.* **1990**, *269* (1), 145−147.
(31) Koppisetti, R. K.; Fulcher, Y. G.; Van Doren, S. R. Fusion Peptide of SARS-CoV-2 Spike Rearranges into a Wedge Inserted in Bilayered Micelles. *J. Am. Chem. Soc.* **2021**, *143* (33), 13205−13211.
(32) Lai, A. L.; Millet, J. K.; Daniel, S.; Freed, J. H.; Whittaker, G. R. The SARS-CoV Fusion Peptide Forms an Extended Bipartite Fusion Platform that Perturbs Membrane Order in a Calcium-Dependent Manner. *J. Mol. Biol.* **2017**, *429* (24), 3875−3892.
(33) Madu, I. G.; Roth, S. L.; Belouzard, S.; Whittaker, G. R. Characterization of a highly conserved domain within the severe acute respiratory syndrome coronavirus spike protein S2 domain with characteristics of a viral fusion peptide. *J. Virol* **2009**, *83* (15), 7411−7421.
(34) Santamaria, A.; Batchu, K. C.; Matsarskaia, O.; Prévost, S. F.; Russo, D.; Natali, F.; Seydel, T.; Hoffmann, I.; Laux, V.; Haertlein, M.; et al. Strikingly Different Roles of SARS-CoV-2 Fusion Peptides Uncovered by Neutron Scattering. *J. Am. Chem. Soc.* **2022**, *144* (7), 2968−2979.
(35) Birtles, D.; Oh, A. E.; Lee, J. Exploring the pH dependence of the SARS-CoV-2 complete fusion domain and the role of its unique structural features. *Protein Sci.* **2022**, *31* (9), No. e4390, DOI: 10.1002/pro.4390.
(36) Birtles, D.; Lee, J. Identifying Distinct Structural Features of the SARS-CoV-2 Spike Protein Fusion Domain Essential for Membrane Interaction. *Biochemistry* **2021**, *60* (40), 2978−2986.
(37) Schaefer, S. L.; Jung, H.; Hummer, G. Binding of SARS-CoV-2 Fusion Peptide to Host Endosome and Plasma Membrane. *J. Phys. Chem. B* **2021**, *125* (28), 7732−7741.
(38) Keating, P. M.; Pennington, H. N.; Collins, S. D.; Lee, J. Purification and characterization of the Lassa virus transmembrane domain. *Biochem Biophys Rep* **2023**, *33*, No. 101409.
(39) Hwang, P. M.; Pan, J. S.; Sykes, B. D. Targeted expression, purification, and cleavage of fusion proteins from inclusion bodies in < i > Escherichia coli</i>. *FEBS Lett.* **2014**, *588* (2), 247−252.
(40) Struck, D. K.; Hoekstra, D.; Pagano, R. E. Use of resonance energy transfer to monitor membrane fusion. *Biochemistry* **1981**, *20* (14), 4093−4099.
(41) Basso, L. G. M.; Zeraik, A. E.; Felizatti, A. P.; Costa-Filho, A. J. Membranotropic and biological activities of the membrane fusion peptides from SARS-CoV spike glycoprotein: The importance of the complete internal fusion peptide domain. *Biochim Biophys Acta Biomembr* **2021**, *1863* (11), No. 183697.
(42) Miles, A. J.; Wallace, B. A. CDtoolX, a downloadable software package for processing and analyses of circular dichroism spectroscopic data. *Protein Sci.* **2018**, *27* (9), 1717−1722.
(43) Shepherd, N. E.; Hoang, H. N.; Abbenante, G.; Fairlie, D. P. Single Turn Peptide Alpha Helices with Exceptional Stability in Water. *J. Am. Chem. Soc.* **2005**, *127* (9), 2974−2983.
(44) Kwok, S. C.; Hodges, R. S. Stabilizing and destabilizing clusters in the hydrophobic core of long two-stranded alpha-helical coiled-coils. *J. Biol. Chem.* **2004**, *279* (20), 21576−21588.
(45) Scheuermann, T. H.; Brautigam, C. A. High-precision, automated integration of multiple isothermal titration calorimetric thermograms: new features of NITPIC. *Methods* **2015**, *76*, 87−98.
(46) Zhao, H.; Piszczek, G.; Schuck, P. SEDPHAT−a platform for global ITC analysis and global multi-method analysis of molecular interactions. *Methods* **2015**, *76*, 137−148.
(47) Brautigam, C. A. Calculations and Publication-Quality Illustrations for Analytical Ultracentrifugation Data. *Methods Enzymol* **2015**, *562*, 109−133.
(48) Matsuo, H.; Chevallier, J.; Mayran, N.; Le Blanc, I.; Ferguson, C.; Fauré, J.; Blanc, N. S.; Matile, S.; Dubochet, J.; Sadoul, R.; et al. Role of LBPA and Alix in multivesicular liposome formation and endosome organization. *Science* **2004**, *303* (5657), 531−534.
(49) Kobayashi, T.; Startchev, K.; Whitney, A. J.; Gruenberg, J. Localization of lysobisphosphatidic acid-rich membrane domains in late endosomes. *J. Biol. Chem.* **2001**, *382* (3), 483−485.
(50) Hu, Y.-B.; Dammer, E. B.; Ren, R.-J.; Wang, G. The endosomal-lysosomal system: from acidification and cargo sorting to neurodegeneration. *Translational Neurodegeneration* **2015**, *4* (1), 18.
(51) Greenfield, N. J. Using circular dichroism spectra to estimate protein secondary structure. *Nat. Protoc* **2006**, *1* (6), 2876−2890.
(52) Manavalan, P.; Johnson, W. C., Jr. Variable selection method improves the prediction of protein secondary structure from circular dichroism spectra. *Anal. Biochem.* **1987**, *167* (1), 76−85.
(53) Whitmore, L.; Wallace, B. A. Protein secondary structure analyses from circular dichroism spectroscopy: Methods and reference databases. *Biopolymers* **2008**, *89* (5), 392−400.
(54) Mant, C. T.; Chen, Y.; Yan, Z.; Popa, T. V.; Kovacs, J. M.; Mills, J. B.; Tripet, B. P.; Hodges, R. S. HPLC analysis and purification of peptides. *Methods Mol. Biol.* **2007**, *386*, 3−55.
(55) Kirchdoerfer, R. N.; Abelson, D. M.; Li, S.; Wood, M. R.; Saphire, E. O. Assembly of the Ebola Virus Nucleoprotein from a Chaperoned VP35 Complex. *Cell Rep* **2015**, *12* (1), 140−149.
(56) Lai, A. L.; Freed, J. H. SARS-CoV-2 Fusion Peptide has a Greater Membrane Perturbating Effect than SARS-CoV with Highly Specific Dependence on Ca(2). *J. Mol. Biol.* **2021**, *433* (10), No. 166946.
(57) Pinto, D.; Fenwick, C.; Caillat, C.; Silacci, C.; Guseva, S.; Dehez, F.; Chipot, C.; Barbieri, S.; Minola, A.; Jarrossay, D.; Tomaras, G. D.; Shen, X.; Riva, A.; Tarkowski, M.; Schwartz, O.; Bruel, T.; Dufloo, J.; Seaman, M. S.; Montefiori, D. C.; Lanzavecchia, A.; Corti, D.; Pantaleo, G.; Weissenhorn, W.; et al. Structural Basis for Broad HIV-1 Neutralization by the MPER-Specific Human Broadly Neutralizing Antibody LN01. *Cell Host Microbe* **2019**, *26* (5), 623−637.e628.
(58) Hulseberg, C. E.; Fénéant, L.; Szymańska, K. M.; White, J. M. Lamp1 Increases the Efficiency of Lassa Virus Infection by Promoting Fusion in Less Acidic Endosomal Compartments. *American Society for Microbiology* **2018**, *9*, 1−14.
(59) Cohen-Dvashi, H.; Cohen, N.; Israeli, H.; Diskin, R. Molecular Mechanism for LAMP1 Recognition by Lassa Virus. *J. Virol* **2015**, *89* (15), 7584−7592.
(60) Li, S.; Sun, Z.; Pryce, R.; Parsy, M. L.; Fehling, S. K.; Schlie, K.; Siebert, C. A.; Garten, W.; Bowden, T. A.; Strecker, T.; et al. Acidic pH-Induced Conformations and LAMP1 Binding of the Lassa Virus Glycoprotein Spike. *PLoS Pathog* **2016**, *12* (2), No. e1005418.
(61) Lüneberg, J.; Martin, I.; Nüssler, F.; Ruysschaert, J. M.; Herrmann, A. Structure and topology of the influenza virus fusion peptide in lipid bilayers. *J. Biol. Chem.* **1995**, *270* (46), 27606−27614.
(62) Das, D. K.; Govindan, R.; Nikić-Spiegel, I.; Krammer, F.; Lemke, E. A.; Munro, J. B. Direct Visualization of the Conformational Dynamics of Single Influenza Hemagglutinin Trimers. *Cell* **2018**, *174* (4), 926−937.
(63) Lai, A. L.; Freed, J. H. HIV gp41 fusion peptide increases membrane ordering in a cholesterol-dependent fashion. *Biophys. J.* **2014**, *106* (1), 172−181.
(64) Villalaín, J. Interaction of Lassa virus fusion and membrane proximal peptides with late endosomal membranes. *Biochim Biophys Acta Biomembr* **2022**, *1864* (11), No. 184031.
(65) Li, Z.; Blissard, G. W. Baculovirus GP64 disulfide bonds: the intermolecular disulfide bond of Autographa californica multicapsid nucleopolyhedrovirus GP64 is not essential for membrane fusion and virion budding. *J. Virol* **2010**, *84* (17), 8584−8595.
(66) Kielian, M. Class II virus membrane fusion proteins. *Virology* **2006**, *344* (1), 38−47.

https://doi.org/10.1021/acsomega.3c08632
ACS Omega 2024, 9, 4920−4930

(67) Lee, J.; Gregory, S. M.; Nelson, E. A.; White, J. M.; Tamm, L. K.; Kuhn, J. H. The Roles of Histidines and Charged Residues as Potential Triggers of a Conformational Change in the Fusion Loop of Ebola Virus Glycoprotein. *Public Library Sci. One* **2016**, *11* (3), 1−14. PubMed
(68) Geney, R.; Layten, M.; Gomperts, R.; Hornak, V.; Simmerling, C. Investigation of Salt Bridge Stability in a Generalized Born Solvent Model. *J. Chem. Theory Comput.* **2006**, *2* (1), 115−127.
(69) Okur, A.; Wickstrom, L.; Simmerling, C. Evaluation of Salt Bridge Structure and Energetics in Peptides Using Explicit, Implicit, and Hybrid Solvation Models. *J. Chem. Theory Comput* **2008**, *4* (3), 488−498.
(70) Barlow, D. J.; Thornton, J. M. Ion-pairs in proteins. *J. Mol. Biol.* **1983**, *168* (4), 867−885.
(71) Sinha, R.; Khare, S. K. Protective role of salt in catalysis and maintaining structure of halophilic proteins against denaturation. *Front Microbiol* **2014**, *5*, 165.
(72) Maity, H.; Muttathukattil, A. N.; Reddy, G. Salt Effects on Protein Folding Thermodynamics. *J. Phys. Chem. Lett.* **2018**, *9* (17), 5063−5070.
(73) Böckmann, R. A.; Hac, A.; Heimburg, T.; Grubmüller, H. Effect of sodium chloride on a lipid bilayer. *Biophys. J.* **2003**, *85* (3), 1647−1655.
(74) Rachakonda, P. S.; Veit, M.; Korte, T.; Ludwig, K.; Böttcher, C.; Huang, Q.; Schmidt, M. F. G.; Herrmann, A. The relevance of salt bridges for the stability of the influenza virus hemagglutinin. *FASEB J.* **2007**, *21* (4), 995−1002.
(75) He, Y.; Liu, S.; Li, J.; Lu, H.; Qi, Z.; Liu, Z.; Debnath, A. K.; Jiang, S. Conserved salt bridge between the N- and C-terminal heptad repeat regions of the human immunodeficiency virus type 1 gp41 core structure is critical for virus entry and inhibition. *J. Virol* **2008**, *82* (22), 11129−11139.
(76) Jiang, S.; Debnath, A. K. A salt bridge between an N-terminal coiled coil of gp41 and an antiviral agent targeted to the gp41 core is important for anti-HIV-1 activity. *Biochem. Biophys. Res. Commun.* **2000**, *270* (1), 153−157.
(77) York, J.; Nunberg, J. H. Intersubunit interactions modulate pH-induced activation of membrane fusion by the Junin virus envelope glycoprotein GPC. *Journal of Virology* **2009**, *83* (9), 4121−4126.
(78) York, J.; Nunberg, J. H. Role of the stable signal peptide of Junín arenavirus envelope glycoprotein in pH-dependent membrane fusion. *Journal of Virology* **2006**, *80* (15), 7775−7780.
(79) York, J.; Dai, D.; Amberg, S. M.; Nunberg, J. H. pH-induced activation of arenavirus membrane fusion is antagonized by small-molecule inhibitors. *J. Virol* **2008**, *82* (21), 10932−10939.
(80) Jasti, J.; Furukawa, H.; Gonzales, E. B.; Gouaux, E. Structure of acid-sensing ion channel 1 at 1.9 A resolution and low pH. *Nature* **2007**, *449* (7160), 316−323.

https://doi.org/10.1021/acsomega.3c08632
ACS Omega 2024, 9, 4920−4930